J|A|C|S COMMUNICATIONS

Published on Web 10/12/2010

Synthesis of Core−Shell Structured Dual-Mesoporous Silica Spheres with Tunable Pore Size and Controllable Shell Thickness

Dechao Niu,[†] Zhi Ma,[‡] Yongsheng Li,*[,†] and Jianlin Shi*[,†,§]

Key Laboratory for Ultrafine Materials of Ministry of Education, School of Materials Science and Engineering, East China University of Science and Technology, Shanghai 200237, China, Shanghai Institute of Organic Chemistry, Chinese Academy of Sciences, Shanghai 200032, China, and State Key Laboratory of High Performance Ceramics and Superfine Microstructure, Shanghai Institute of Ceramics, Chinese Academy of Sciences, Shanghai 200050, China

Received August 6, 2010; E-mail: ysli@ecust.edu.cn; jlshi@sunm.shcnc.ac.cn

Abstract: Core−shell structured dual-mesoporous silica spheres (DMSS) that possess smaller pores (2.0 nm) in the shell and larger tunable pores (12.8−18.5 nm) in the core have been successfully synthesized by utilizing an amphiphilic block copolymer (polystyrene-*b*-poly (acrylic acid), PS-*b*-PAA) and cetyl trimethyl ammonium bromide (CTAB) as cotemplates. The thickness of the shells and the larger pore size in the core could be easily tuned by changing the amounts of TEOS and the hydrophobic block (PS) length during synthesis, respectively. By encapsulating hydrophobic magnetite nanoparticles into the cores, superparamagnetic dual-mesoporous silica spheres were obtained. Drug storage and release testing results showed that the diffusing rate of the stored drug could be efficiently controlled by changing the shell thickness of DMSS.

Hierarchically porous materials with multimodal pore systems have attracted increasing attention because of their unique, adjustable, and well-defined pore structure and great potential for applications in catalysis, sorption, separation, and biomedical fields.[1] Up to now, various templating approaches have been adopted to synthesize hierarchically porous materials by using emulsions, colloids, and surfactants as templates.[2−4] Especially, hierarchically porous materials with bimodal mesoporosity can be synthesized by a "dual templating" approach or chemical and hydrothermal post-treatments of mesoporous silica materials.[5] However, in all these cases, structural control was difficult, and most of these bimodal mesoporous materials lack a well-defined pore structure on at least one length scale in terms of pore shape or size. In addition, the macropore sizes were usually large, at least at 200−300 nm, though smaller macropores (<100 nm) would be more desirable.[6] Recently, a novel kind of hierarchically bimodal mesopore materials with tunable pore size and structure has been synthesized successfully by using various block copolymers as a large pore template and a smaller surfactant as a small pore template;[7] however, the obtained particles suffered from the irregular morphology and broadened particle size distribution. Consequently, developing a novel approach on the synthesis of dual-mesoporous materials with well-defined particle morphology and size in the nanoscale (∼200 nm) is still a great challenge.

Herein, we report a very simple method on the synthesis of core−shell structured and monodispersed dual-mesoporous silica spheres (designated as DMSS) with larger pores in the core and smaller pores in the shell using amphiphilic block copolymer polystyrene-*b*-poly (acrylic acid) (PS-*b*-PAA) and cetyltrimethylammonium bromide (CTAB) as dual templates. Different from previously reported block copolymer-templating methods,[8] anionic block copolymer PS-*b*-PAA is used in the present study as a template to form the larger mesopores. More importantly, the size of the larger pores and the thickness of the shell can be easily tuned by changing the length of PS blocks of PS-*b*-PAA and the precursor composition, respectively (Table S1). It is important to note that dual-mesoporous silica spheres prepared by this method have uniform particle sizes and a well-defined core−shell structure. Also, functional dual-mesoporous silica spheres were successfully prepared by encapsulating hydrophobic nanoparticles (such as magnetic Fe_3O_4 particles) in the large pores. Drug storage and release testing results showed that up to 500 mg of ibuprofen could be stored in 1 g of DMSS, and the diffusion rate of drug molecules can be effectively tuned by varying the thickness of the shell.

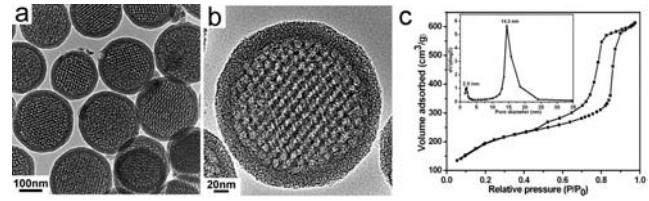

Figure 1. TEM images (a, b) as well as N_2 adsorption−desorption isotherms and BJH pore diameter distribution curve at adsorption branch (inset) (c) of DMSS-PS_{100}.

Figure 1a presents typical TEM images of DMSS prepared with block copolymer PS_{100}-*b*-PAA_{16} as one template (denoted as DMSS-PS_{100}). Well-defined core−shell structured nanospheres of ∼250 nm in diameter are clearly presented. It is interesting to note that the core is neither solid nor hollow but is composed of ordered mesopores with a pore diameter of around 14 nm. An HRTEM image of DMSS-PS_{100}, as shown in Figure 1b, further confirms the core−shell structured dual-mesoporous structure with larger pores in the core and smaller pores (∼2.0 nm) in the shell. In order to confirm the mesostructural ordering, small angle X-ray scattering (SAXS) analysis was adopted (Figure S1). As shown in Figure S1, the SAXS pattern of DMSS-PS_{100} shows well-resolved scattering peaks in the q range 0.03−0.13 A^{-1}, indicating an ordered hexagonal mesostructure in the cores. In addition, the XRD pattern of DMSS-PS_{100} shown in Figure S2 also indicates the ordered arrangement of the larger mesopores. However, the broadened scattering peak in the q range 0.15−0.20 A^{-1} in Figure S1 and the equally broadened diffraction peak in the 2θ range 2°−3° show the disordered arrangement of the smaller mesopores, which is also in accordance with the above TEM observations (Figure 1b). In

[†] School of Materials Science and Engineering, East China University of Science and Technology.
[‡] Shanghai Institute of Organic Chemistry, Chinese Academy of Sciences.
[§] Shanghai Institute of Ceramics, Chinese Academy of Sciences.

 10.1021/ja1070653

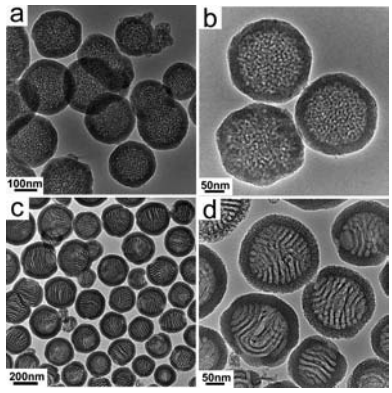

Figure 2. TEM images of DMSS prepared by using block copolymers of different lengths of PS block as templates: (a, b) PS_{78}-*b*-PAA_{16}, (c, d) PS_{154}-*b*-PAA_{16}.

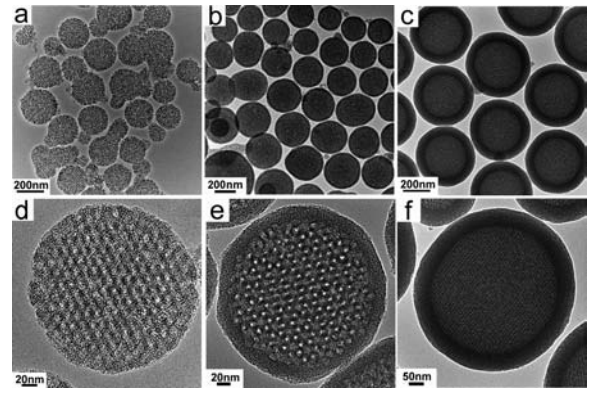

Figure 3. TEM images of DMSS with different shell thicknesses: (a, d) 5 nm, (b, e) 25 nm, and (c, f) 60 nm.

Scheme 1. Schematic Illustration for the Formation of Dual-Mesoporous Silica Spheres[a]

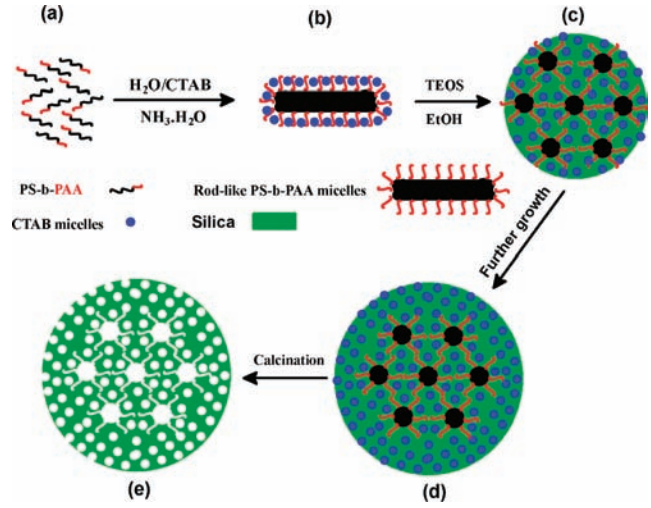

[a] (a) THF solution of PS-*b*-PAA; (b) CTAB-coated PS-*b*-PAA aggregates formed by the electrostatic interaction between CTA^+ and PAA^-; (c) Core part formed from the assembly between CTAB-coated PS-*b*-PAA aggregates and TEOS; (d) Mesoporous shell formation via the self-assembly between the remaining CTAB and the additional TEOS; (e) Final core-shell structured dual-maeoporous silica spheres after calcination.

order to understand the dual-mesoporous structure of DMSS more clearly, an HRTEM image (Figure S3) of an ultrathin microtome section of DMSS-PS_{100} was examined. It should also be noted that smaller mesopores are present not only in the shells but also in the large pore framework in the cores, while larger mesopores can only be found in the cores.

In order to further demonstrate the dual-mesoporous structure of DMSS-PS_{100}, N_2 sorption analysis was performed (Figure 1c). As shown in Figure 1c, the adsorption−desorption isotherms show two major capillary condensation steps in the relative pressure ranges 0.1−0.3 and 0.80−0.95, implying that two sets of mesopores respectively at ∼2.0 nm and ∼14 nm in diameter have been obtained as can be identified from the corresponding distribution curve of DMSS-PS_{100}, which is obtained by the Barrett−Joyner−Halenda (BJH) method. In addition, the specific surface area and total volume of DMSS-PS_{100} is calculated to be 697 $m^2 \cdot g^{-1}$ and 0.95 $cm^3 \cdot g^{-1}$, respectively. Noticeably, it is known that the BJH method is quite good for large pores but may underestimate the size of small pores. As the CTAB-templated mesopores are usually small in the range 3−3.5 nm, to obtain a more accurate pore size, a novel nonlocal density functional theory (NLDFT) method was used for the calculation of pore size and distribution from adsorption isotherms.[9] As shown in Figure S4, the smaller pore size of DMSS-PS_{100} by the NLDFT method is around 2.94 nm. Therefore, the small pores in our DMSS in the present work can be underestimated by about 1 nm by the BJH method.

Under similar conditions to those for DMSS-PS_{100}, DMSS with varied larger pore sizes, i.e. DMSS-PS_{78}, DMSS-PS_{154}, and DMSS-PS_{260}, were obtained by changing the length of the PS block. TEM images together with the N_2 sorption analysis results demonstrate the core−shell dual-mesoporous structure and spherical morphology of DMSS-PS_{78} and DMSS-PS_{154} (Figures 2 and S5). On increasing the number of PS block units in PS-*b*-PAA from 78 to 154, the larger pore diameter in the cores was enlarged from 12.8 to 18.5 nm, respectively, while the smaller mesopores keep constant at about 2.0 nm. This means that the number of PS blocks determines the larger pore size of DMSS, to a large extent. However, mesoporous hollow silica spheres were obtained with the number of PS block units increasing to 260 (Figures S5 and S6). Such a change of particle structure can be most probably attributed to the micelle morphology transformation from rod-like to vesicle or other large compound micelles. As amphiphilic block copolymer PS-*b*-PAA may form micelles of varied morphologies (e.g., spherical, rod-like, vesicle, and large compound micelles),[10] it is anticipated that various particle morphologies of different hierarchical pore structures could be prepared with the present methodology. In addition, the shell thickness of DMSS could be well adjusted by changing the amount of TEOS during synthesis. As shown in Figures 3 and S7, the shell thickness of DMSS-PS_{100} could be varied in the range 5 to 60 nm, with the particle size varying from 200 to 400 nm, correspondingly.

Based on the above observations, a possible mechanism was proposed to explain the formation of dual-mesoporous silica spheres (Scheme 1). As the morphology of PS-*b*-PAA micelles could be changed from spheres to rod-like aggregates by the addition of inorganic ions or small molecule surfactants,[11] in our experiments, rod-like aggregates were assumed to form in the presence of a small molecule surfactant (CTAB) and ammonia (NH_4^+) at the beginning stage, which was confirmed by the TEM observation of a precursor solution before adding ethanol and TEOS (Figure S8). At the same time, the hydrophilic PAA blocks of rod-like aggregates could couple with the CTAB micelles via Coulomb force and electrostatic interaction between CTA^+ and PAA^- to form CTAB-coated rod-like aggregates, or composite micelles, in solution. After the addition of TEOS and ethanol, the inorganic−organic self-assembled hybrid micelles, which are composed of silicate oligomers and CTAB-coated PS-*b*-PAA rod-like aggregates, were first formed. Then, these

rod-like silicate composite micelles pack together in an ordered fashion to form the core part dual-mesoporous structure, which is similar to the model proposed by Cai and co-workers.[12] Finally, the electrostatic interaction between positively charged CTA^+ and negatively charged silica species and the condensation of the rod-like silicate micelles facilitate the deposition of the micelles, resulting in the formation of mesoporous silica with a spherical morphology. As a certain limited amount of CTAB can coat the PS-*b*-PAA micelles to form composite micelles, the remaining CTAB molecules will be expelled out of the core portion of the structure, and once the core part becomes large enough, the immediate outer region of the core (or, the interface between the core and the liquid phase) will become sufficiently rich in CTAB, leading to the cooperative self-assembly between these CTAB molecules and additional TEOS and consequently the formation of an outer shell of smaller pores surrounding the cores.

From this proposed mechanism, it is clear that CTAB plays an important role in the formation of the structure. Without CTAB, CTAB-coated PS-*b*-PAA aggregates cannot form and the corresponding self-assembly between the CTAB-coated PS-*b*-PAA aggregates and TEOS could not take place, so that mesoporous materials will not be obtained. In addition, ethanol solvent plays an essential role in the formation of stable CTAB-coated rod-like aggregates. As shown in Figure S9, without or with the addition of a small amount of ethanol (e.g., 40 mL), dual-mesoporous silica spheres cannot be obtained; only conventional mesoporous silica spheres with a single pore system at 2.3 nm, or sometimes with few large pore channels, were formed. In contrast, when a much larger amount of ethanol (120 mL) was employed, only large-pore mesoporous silica spheres with a pore size of 15 nm were observed. The reason for the disappearance of smaller pores is probably due to the largely increased critical micelle concentration (CMC) of CTAB with the increased amount of ethanol,[13] which is higher than that of CTAB micelle concentration, resulting in the dissociation of CTAB micelles. This transformation was also confirmed by N_2 sorption analysis (Figure S10).

In addition, this method also provides opportunities for developing dual-mesoporous silica spheres with specific functions. Here, we demonstrated the successful incorporation of magnetite nanoparticles into the larger pores of DMSS for magnetic functionalization. From the TEM images of magnetite-loaded dual-mesoporous silica spheres (denoted as Fe_3O_4@DMSS, Figure S11), it can be seen that the monodispersity and dual-mesoporous structure of particles were not affected with the encapsulation of magnetite nanoparticles. Due to the small size of magnetite nanoparticles (~4 nm), it is hard to distinguish the Fe_3O_4 nanoparticles from the matrix in the TEM image. However, the energy dispersive spectrum (EDS) and XRD pattern of Fe_3O_4@DMSS confirm the existence of Fe_3O_4 nanoparticles in the particles (Figures S12 and S13). N_2 adsorption−desorption analysis (Figure S14) shows two sets of mesopores centered at 2.1 and 11.2 nm, respectively, and a high specific surface area of 1154 $m^2 \cdot g^{-1}$ and pore volume of 1.21 $cm^3 \cdot g^{-1}$ were obtained for Fe_3O_4@DMSS. The magnetic properties of Fe_3O_4@DMSS at 300 K were recorded using a vibrating-sample magnetometer (VSM), as presented in Figure S11c, demonstrating their superparamagnetic feature with a saturation magnetization value of 2.5 emu/g, which is desirable for their biomedical applications, such as in magnetic separation, magnetic resonance imaging (MRI), targeted drug delivery, and hyperthermia treatment of cancer.[14] The magnetic separability of Fe_3O_4@DMSS was further visually tested in water by placing a magnet near the glass bottle. The particles were attracted toward the magnet within several minutes, as shown in Figure S11d, demonstrating directly that the core−shell nanospheres have been endowed with magnetic properties. Following the same procedure, various kinds of hydrophobic nanoparticles can be encapsulated in the core of the dual-mesoporous silica spheres, resulting in multifunctional silica spheres with the dual-mesoporous structure.

To explore its capability as a drug carrier, ibuprofen, a typical anti-inflammatory drug, was introduced into the pores of DMSS of varied shell thicknesses of 5, 25, and 60 nm and denoted as $DMSS_{100}$-ST5, $DMSS_{100}$-ST25, and $DMSS_{100}$-ST60, respectively. The uptake amounts of ibuprofen are ca. 26.3, 34.6, and 29.5 wt %, as assessed by TG analysis. The release behavior of ibuprofen in PBS solution (pH = 7.4) was measured over a 24 h period (Figure S15). It is clear that the release rates of drug molecules could be controlled by changing the shell thickness of DMSS. In addition, an apparent three-stage ibuprofen release profile from samples $DMSS_{100}$-ST25 and $DMSS_{100}$-ST60 is clear: the first stage involves the rapid release of ibuprofen within the first 60 min, owing to the release of IBU adsorbed on the external surface. Then, the release amount of ibuprofen increases again from 2 to 6 h and reaches a plateau at 73% for sample $DMSS_{100}$-ST25, for example. It is reasonable to attribute this release to those trapped in the small pore. Finally, the ibuprofen concentration increases from 6 to 24 h and eventually reaches another plateau at 80% for $DMSS_{100}$-ST25. The release in the last stage could probably be attributed to the adsorbed drug in the large pores. The three-step release profile of the dual-mesoporous structure is similar with that for mesoporous and yolk-shell structure reported previously.[15] This indicates that DMSS can be an effective carrier for drug deliver and release.

In summary, a novel kind of core−shell structured dual-mesoporous silica spheres with a hierarchical pore structure, which are composed of smaller mesopores in the shells and ordered larger mesopores in the cores, have been fabricated by a simple dual-templating method. The larger pore size of DMSS can be easily tuned by changing the PS block length of PS-*b*-PAA. In addition, the shell thickness of dual-mesoporous silica spheres can be well controlled from 5 to 60 nm by varying the concentration of TEOS. A three-step release profile of drugs was observed with these particular dual-mesoporous structures. Also, superparamagnetic magnetite nanoparticles can be encapsulated in dual-mesoporous silica spheres, resulting in functionalized composite spheres, which may find potential applications in catalysis, sorption, separation, and biomedical fields.

Acknowledgment. This work was financially supported by the National Hi-Tech Project of China (Grant No. 2007AA03Z317); the National Natural Science Foundation of China (Grant No. 20633090 and 21001043), Scientific Innovation Project of Shanghai Municipal Education Commission (Grant No. 11ZZ53), and Shanghai Pujiang Program (Grant No. 09PJ1403000).

Supporting Information Available: Experimental details for the synthesis and additional figures. This material is available free of charge via the Internet at http://pubs.acs.org.

References

(1) (a) Dong, A. G.; Wang, Y. J.; Tang, Y.; Zhang, Y. H.; Ren, N.; Gao, Z. *Adv. Mater.* **2002**, *14*, 1506–1510. (b) Li, Y. S.; Shi, J. L.; Hua, Z. L.; Chen, H. R.; Ruan, M. L.; Yan, D. S. *Nano Lett.* **2003**, *3*, 609–612. (c) Chen, H.; Shi, J.; Li, Y.; Yan, J.; Hua, Z.; Chen, H.; Yan, D. *Adv. Mater.* **2003**, *15*, 1078–1081. (d) Brandhuber, D.; Torma, V.; Raab, C.; Peterlik, H.; Kulak, A.; Husing, N. *Chem. Mater.* **2005**, *17*, 4262–4271. (e) Mori, H.; Uota, M.; Fujikawa, D.; Yoshimura, T.; Kuwahara, T.; Sakai, G.; Kijima, T. *Microporous Mesoporous Mater.* **2006**, *91*, 172–180. (f) Kuang, D. B.; Brezesinski, T.; Smarsly, B. *J. Am. Chem. Soc.* **2004**, *126*, 10534–10535.

(2) (a) Sen, T.; Tiddy, G. J. T.; Casci, J. L.; Anderson, M. W. *Chem. Commun.* **2003**, 2182–2183. (b) Wang, J. G.; Xiao, Q.; Zhou, H. J.; Sun, P. C.; Yuan,

Z. Y.; Li, B. H.; Ding, D. T.; Shi, A. C.; Chen, T. H. *Adv. Mater.* **2006**, *18*, 3284–3288. (c) Feng, Z. G.; Li, Y. S.; Niu, D. C.; Li, L.; Zhao, W. R.; Chen, H. R.; Gao, J. H.; Ruan, M. L.; Shi, J. L. *Chem. Commun.* **2008**, 2629–2631.
(3) (a) Antonietti, M.; Berton, B.; Göltner, C.; Hentze, H. *Adv. Mater.* **1998**, *10*, 154–159. (b) Stein, A.; Li, F.; Denny, N. R. *Chem. Mater.* **2008**, *20*, 649–666. (c) Chen, X.; Sun, Z. Q.; Zheng, L. L.; Chen, Z. M.; Wang, Y. F.; Fu, N.; Zhang, K.; Yan, X.; Liu, H.; Jiang, L.; Yang, B. *Adv. Mater.* **2004**, *16*, 1632–1636.
(4) (a) Suzuki, K.; Ikari, K.; Imai, H. *J. Mater. Chem.* **2003**, *13*, 1812–1816. (b) Sun, J.; Shan, Z.; Maschmeyer, T.; Coppens, M. O. *Langmuir* **2003**, *19*, 8395–8402. (c) Ikari, K.; Suzuki, K.; Imai, H. *Langmuir* **2004**, *20*, 11504–11508. (d) Groenewolt, M.; Antonietti, M. *Langmuir* **2004**, *20*, 7811–7819. (e) Sen, T.; Tiddy, G. J. T.; Casci, J. L.; Anderson, M. W. *Angew. Chem., Int. Ed.* **2003**, *42*, 4649–4653. (f) Niu, D. C.; Li, Y. S.; Dong, W. J.; Zhao, W. R.; Li, L.; Shi, J. L. *J. Mater. Sci.* **2009**, *44*, 6519–6524.
(5) (a) Wang, X.; Dou, T.; Xiao, Y. *Chem. Commun.* **1998**, 1035–1036. (b) Bagshaw, S. A. *Chem. Commun.* **1999**, 1785–1786. (c) Sun, J.; Shan, Z.; Maschmeyer, T.; Moulijn, J. A.; Coppens, M. O. *Chem. Commun.* **2001**, 2670–2671. (d) El Haskouri, J.; de Zarate, D. O.; Guillem, C.; Latorre, J.; Caldes, M.; Beltran, A.; Beltran, D.; Descalzo, A. B.; Rodriguez, G.; Martinez-Manez, R.; Marcos, M. D.; Amoros, P. *Chem. Commun.* **2002**, 330–331. (e) Yuan, Y.; Blin, J. L.; Su, B. L. *Chem. Commun.* **2002**, 504–505. (f) Okabe, A.; Niki, M.; Fukushima, T.; Aida, T. *J. Mater. Chem.* **2005**, *15*, 1329–1331.
(6) Yang, P.; Deng, T.; Zhao, D.; Feng, P.; Pine, D.; Chmelka, B. F.; Whitesides, G. M.; Stucky, G. D. *Science* **1998**, *282*, 2244–2246.
(7) Sel, O.; Kuang, D.; Thommes, M.; Smarsly, B. *Langmuir* **2006**, *22*, 2311–2322.
(8) Ryoo, R.; Ko, C. H.; Kruk, M.; Antochshuk, V.; Jaroniec, M. *J. Phys. Chem. B* **2000**, *104*, 11465–11471.
(9) (a) Ravikovitch, P. I.; Wei, D.; Chueh, W. T.; Haller, G. L.; Neimark, A. V. *J. Phys. Chem. B* **1997**, *101*, 3671–3679. (b) Kruk, M.; Jaroniec, M. *Chem. Mater.* **2001**, *13*, 3169–3183.
(10) Shen, H. W.; Eisenberg, A. *Macromolecules* **2000**, *33*, 2561–2572.
(11) (a) Yu, Y.; Zhang, L.; Eisenberg, A. *Macromolecules* **1998**, *31*, 1144–1154. (b) Zhang, L.; Yu, K.; Eisenberg, A. *Science* **1996**, *272*, 1777–1779. (c) Zhang, L.; Eisenberg, A. *Macromolecules* **1996**, *29*, 8805–8815. (d) Yu, Y.; Eisenberg, A. *J. Am. Chem. Soc.* **1997**, *119*, 8383–8384.
(12) Cai, Q.; Luo, Z.; Pang, W.; Fan, Y.; Chen, X.; Cui, F. *Chem. Mater.* **2001**, *13*, 258–263.
(13) (a) Tan, B.; Rankin, S. E. *J. Phys. Chem. B* **2004**, *108*, 20122–20129. (b) Nazira, N.; Ahangera, M. S.; Akbar, A. *J. Dispersion Sci. Technol.* **2009**, *30*, 51–55.
(14) (a) Jeong, U.; Teng, X.; Wang, Y.; Yang, H.; Xia, Y. *Adv. Mater.* **2007**, *19*, 33–60. (b) Gu, H.; Xu, K.; Xu, C.; Xu, B. *Chem. Commun.* **2006**, 941–949. (c) Hu, F.; Wei, L.; Zhou, Z.; Ran, Y.; Li, Z.; Gao, M. *Adv. Mater.* **2006**, *18*, 2553–2556. (d) Veiseh, O.; Sun, C.; Gunn, J.; Kohler, N.; Gabikian, P.; Lee, D.; Bhattarai, N.; Ellenbogen, R.; Sze, R.; Hallahan, A.; Olson, J.; Zhang, M. *Nano Lett.* **2005**, *5*, 1003–1008. (e) Nasongkla, N.; Bey, E.; Ren, J.; Ai, H.; Khemtong, C.; Guthi, J. S.; Chin, S.; Sherry, A. D.; Boothman, D. A.; Gao, J. *Nano Lett.* **2006**, *6*, 2427–2430. (f) Niu, D. C.; Li, Y. S.; Ma, Z.; Diao, H.; Gu, J. L.; Zhao, W. R.; Chen, H. R.; Ruan, M. L.; Zhang, Y. L.; Shi, J. L. *Adv. Funct. Mater.* **2010**, *20*, 773–780.
(15) Liu, J.; Qiao, S. Z.; Hartono, S. B.; Lu, G. Q. *Angew. Chem., Int. Ed.* **2010**, *49*, 4981–4985.

JA1070653